Multiorgan characterization of inflammasome component expression in a rat model of advanced heart failure

Dávid Nagy^{1,2}, Zsófia Onódi^{3,4,5}, Márton Kocsis^{3,4,5}, Artúr Tóth^{3,4,5}, Tímea Bálint^{1,2}, Attila Oláh^{1,2}, Alex Ali Sayour^{1,2}, Bálint András Barta^{1,2}, Béla Merkely¹, Péter Ferdinandy^{3,6}, Tamás Radovits^{1,2}, Zoltán V. Varga^{3,4,5} and Mihály Ruppert^{1,2*}

¹Department of Cardiology, Heart and Vascular Center, Semmelweis University, Budapest, Hungary; ²Department of Experimental Cardiology and Surgical Techniques, Heart and Vascular Center, Semmelweis University, Budapest, Hungary; ³Department of Pharmacology and Pharmacotherapy, Center for Pharmacology and Drug Research and Development, Semmelweis University, Budapest, Hungary; ⁴HCEMM-SU Cardiometabolic Immunology Research Group, Budapest, Hungary; ⁵MTA-SE Momentum Cardio-Oncology and Cardioimmunology Research Group, Semmelweis University, Budapest, Hungary; and ⁶Pharmahungary Group, Szeged, Hungary

Abstract

Aims Targeting inflammasomes in heart failure (HF) might represent a novel therapeutic option. Nevertheless, previous studies focused only on myocardial inflammasome alterations, and data are scarce regarding their regulation and role in HF-associated multiorgan dysfunction. Therefore, we aimed to determine the myocardial, pulmonary, hepatic and renal expression of various inflammasome components in a rat model of advanced HF.

Methods and results Rats underwent transverse aortic constriction (TAC) and were followed-up for 15 weeks. Animals featuring two to three clinical signs of advanced HF were included in the TAC-HF group (n = 6). TAC rats with mild HF were also investigated (0–1 signs, TAC-M group, n = 6). Six sham-operated animals served as controls. The expressions of inflammasome component proteins in left ventricle (LV), right ventricle (RV), lung, liver and kidney tissue were measured with Western blot. Despite the differences between the clinical state of the TAC-HF and TAC-M groups, severe cardiac dysfunction and myocardial remodelling developed in all TAC animals. Absent in melanoma 2 (AIM2) and NLR family CARD domain-containing protein 4 (NLRC4) inflammasome sensors were up-regulated in both the LV and RV of the TAC-HF group compared with sham. AIM2 and NLR family pyrin domain-containing protein 3 (NLRP3), but not NLRC4 expression were elevated in the lungs of the TAC-HF animals. Additionally, pulmonary congestion and CD68-positive leukocyte infiltration were observed in both TAC groups. Inflammasome components were down-regulated in the liver and remained unchanged in the kidneys of the TAC-HF group, despite the presence of renal atrophy and fibrosis. Inflammasome changes were predominantly absent in TAC-M animals.

Conclusions Inflammasome expression shows distinct patterns in specific organs in advanced HF. Future studies aiming to antagonize inflammation in HF should take these findings into consideration.

Keywords Absent in melanoma 2; Advanced heart failure; End-organ damage; NLR family CARD domain-containing protein 4; NLR family pyrin domain-containing protein 3; Inflammasome

Received: 10 December 2024; Revised: 29 May 2025; Accepted: 16 June 2025

*Correspondence to: Mihály Ruppert, Department of Experimental Cardiology and Surgical Techniques Heart and Vascular Center, Semmelweis University, Városmajor u. 68., 1122 Budapest, Hungary. Email: ruppert.mihaly@semmelweis.hu

Dávid Nagy and Zsófia Onódi contributed equally as first authors.

Zoltán V. Varga and Mihály Ruppert contributed equally as last authors.

Introduction

Despite the rapidly developing therapeutic options over the past decades, the incidence and mortality of heart failure

(HF) still remain high in the general population. Advanced HF—a clinical state with refractory symptoms despite optimal medical therapy—has especially poor prognosis. Advanced HF can often culminate into multiorgan dysfunction as well.

The impairment of extracardiac organs can drive the clinical progression independently of cardiac function, thus impacting long-term survival and limiting therapeutic options. The interplay of the heart and other organs in HF is still under extensive investigations. Pathological haemodynamic conditions lead to the congestion and/or hypoperfusion of end-organs, which initiates several intertwining maladaptive mechanisms. One of the best characterized among them is neurohormonal activation, which includes increased sympathetic tone and the stimulation of the reninangiotensin-aldosterone system. Current pharmacological therapy of HF with reduced ejection fraction (HFrEF) aims to mitigate these alterations predominantly.

Besides neurohormonal changes, elevated levels of inflammatory markers are long-known characteristics of HF as well.^{7,8} All recent evidence points in the direction that systemic inflammation is not only a response to injury in HF but also a causative factor of further decline. In preclinical settings, therapeutic targeting of inflammation in HF has been found to successfully improve survival. 10 Most clinical trials on larger sample sizes however, failed to replicate these results. 11,12 The only promising direction seems to be the antagonization of interleukin-1 beta (IL-1\beta), based on the favourable cardiovascular outcomes of the CANTOS trial and its substudies. $^{13-15}$ On the other hand, IL-1 β blockade also increased the incidence of fatal infections, and all-cause mortality was eventually unchanged in the study population. This suggests the need for a more specific intervention in the complex inflammatory processes. IL-1ß is activated exclusively through the inflammasome pathway. 16 Inflammasomes are intracellular pathogen- or danger-sensing multiprotein complexes of the innate immune system, expressed most abundantly by monocytes/macrophages. 17 Multiple inflammasome receptor proteins exist, each of them responds to different types of molecular patterns. 17 Besides the diverse sensors, all types of inflammasomes include a common adapter molecule (apoptosis-associated speck-like protein containing a CARD, ASC) and activate caspase-1 finally. 17 Gasdermin D (GSDMD), IL-1 β and interleukin-18 (IL-18) are the downstream targets of caspase-1.¹⁷

Because several upstream inflammasome sensors that respond to different stimuli exist, modulating them would be a feasible alternative therapeutic approach. Numerous experiments in the cardiovascular field—including HF—confirm this notion. ^{18,19} Dapansutrile, a selective oral inhibitor of NLR family pyrin domain-containing protein 3 (NLRP3), has shown promising results in a phase 1B clinical trial on HFrEF patients. ²⁰ The role of inflammasomes is well-established in various types of extracardiac organ dysfunction as well. ^{21,22} Cytokines and inflammasomes were also examined in certain organ interactions accompanying HF. ^{23–25} However, the expression of inflammasomes in advanced HF-associated multiorgan failure has not been comprehensively characterized yet.

Our study aimed to characterize the left- and right ventricular (LV and RV, respectively) and extracardiac (lung, kidney and liver) expression of relevant inflammasome elements in a rat model of pressure overload-induced HF. In this regard, we intended to compare the advanced, symptomatic and the asymptomatic HF phenotypes in an otherwise similar population.

Methods

See the extended version of the description of experimental materials and methods in Section S1 and *Tables* S1 and S2.

Ethical approval

The experimental animals (male Wistar rats, 50–75 g) were treated according to the 'Principles of Laboratory Animal Care' established by the National Society for Medical Research and the 'Guide for the Care and Use of Laboratory Animals' prepared by the Institute of Laboratory Animal Resources and published by the US National Institutes of Health (NIH Publication no. 86-23, revised 1996). The investigation conforms to the EU Directive (2010/63/EU). Approval for the study was obtained from the animal ethics committee of Semmelweis University, Budapest, Hungary (PEI/001/2374-4/2015). The results are interpreted in accordance with the *Animal Research: Reporting of In Vivo Experiments* (ARRIVE) guidelines.

Transverse aortic constriction model

After a one-week long acclimatization period, rats underwent transverse aortic constriction (TAC) surgery, as described elsewhere. In short, left anterolateral thoracotomy was performed under isoflurane anaesthesia. The aorta was constricted to a size of a 21-gauge needle between the brachiocephalic trunk and the left common carotid artery. The sham operation was identical to the TAC surgery, except the aortic constriction step of the protocol.

Experimental groups and study design

Based on previous experience with the model, we expected advanced HF to develop in at least a subset of animals by the 16th week post-TAC operation. Ultimately, some animals progressed to cardiac decompensation and were terminated earlier. The median follow-up time was 15 weeks, with a range of 14 to 16 weeks. As the focus of this study is advanced HF as a clinical state (which is often independent of cardiac function), we applied a simple scoring method at

the end of the follow-up period to form our three study groups from the TAC- and sham-operated rats (see Table Material 1.3. and *Table* S1).

In vivo measurements and tissue collection

At the end of the follow-up period, echocardiography and LV pressure-volume (P-V) analysis were carried out under isoflurane anaesthesia according to our previously described protocol.²⁷ The abdominal aorta was cannulated immediately after the P-V measurements and the animals were euthanized by exsanguination. During this process, arterial blood samples were also collected into serum clot activator or EDTA tubes for serum or plasma samples, respectively. After centrifugation, the supernatant serum and plasma samples were aliquoted and stored at -80°C. Oxygenated Ringer solution (50 mL) was infused retrogradely after the termination of the animal was confirmed based on the ECG recordings. Hearts, lungs, livers and kidneys were harvested and placed immediately into 4°C Ringer solution. After organ weight measurements, 40-50 mg pieces of LV, RV, lung, liver and kidney tissue were sampled and immediately snap-frozen in liquid nitrogen and stored at -80°C for the molecular analyses. A cross section of the hearts (at the level of the ventricles) and 1 cm × 1 cm pieces of the other organs were placed in 4% buffered paraformaldehyde for the histological analyses as well.

In vitro measurements

In vitro measurements from the conserved samples were performed as previously described.²⁸ Fibrosis area was measured on picrosirius red-stained LV, RV, lung, liver and kidney histological sections. Immunohistochemistry was used to determine CD68-positive cell count in the lung and liver specimens. Inflammasome component expressions in the LV, RV, lung, liver and kidney were assessed with Western immunoblotting. Circulating markers of liver function (albumin; AST, aspartate aminotransferase; ALT, alanine aminotransferase; total bilirubin) were measured in the clinical routine diagnostic laboratory of Semmelweis University Heart and Vascular Center (Budapest, Hungary) from frozen serum and plasma samples. Plasma N-terminal prohormone of brain natriuretic peptide (NT-proBNP) concentration was assessed using rat N-terminal pro-brain natriuretic peptide, NT-proBNP ELISA KIT (#CSB-E08752r; Cusabio Technology, Houston, TX, USA) according to the manufacturer's protocol.

Statistical analysis

All values are expressed as mean ± standard error of the mean. The distribution of the datasets was tested by the Shapiro–Wilk normality test. One-way analysis of variance

(ANOVA) followed by Tukey's post hoc test were carried out in case of normal distribution, Kruskal–Wallis test followed by Dunn's post hoc test were used in case of non-normal distribution to compare the three study groups. A *P* value of <0.05 was considered statistically significant. Statistical analysis was performed with GraphPad Prism 8 (GraphPad Software Inc., San Diego, CA, USA).

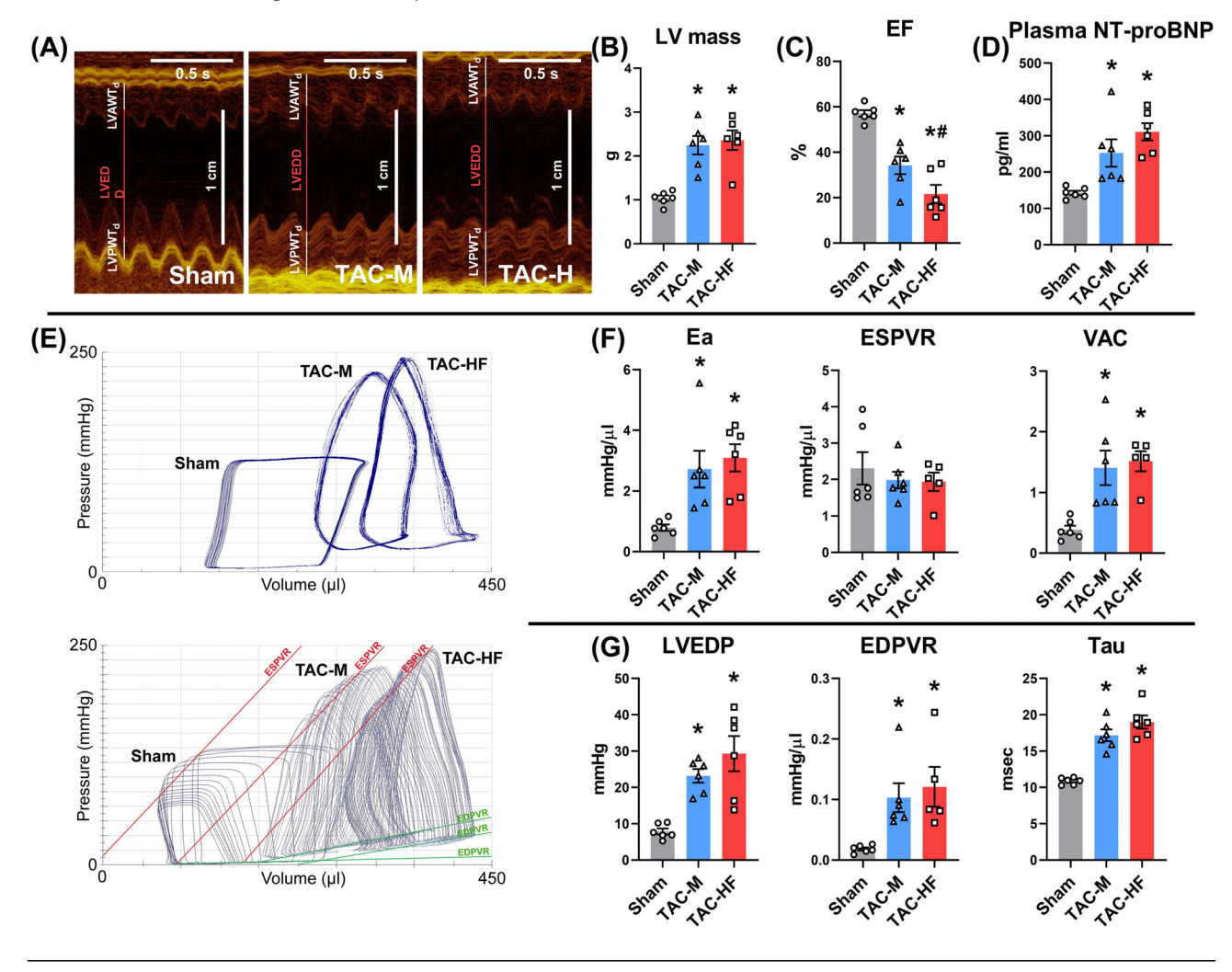
Results

Characterization of the TAC model

According to the measured cardiac functional parameters, both TAC-M and TAC-HF groups featured severe systolic and diastolic LV dysfunction. The average of the ejection fraction (EF) calculated from the parameters obtained during the P-V measurements decreased below 40% in both TAC groups (Figure 1C). NT pro-BNP, widely used in clinical settings to monitor disease severity in HF patients, was also found to be higher in all TAC animals compared with the controls (Figure 1D). Arterial and LV systolic pressures (see Table 1) were greater in the aortic constricted rats, indicating profoundly elevated afterload. LV contractility failed to compensate the increment in afterload, which was demonstrated by the impairment of ventriculo-arterial coupling ratio (Figure 1E,F). Moreover, the differences in the maximal velocity and the time constant of LV pressure decline (dPdt_{min} and Tau, respectively) in the TAC-M and TAC-HF animals reveal the disturbance of LV active relaxation in the diastole (Figure 1G, Table 1). Passive filling of the LV was also impaired in these groups, as evidenced by the elevated LV end-diastolic pressure (LVEDP) and slope of end-diastolic pressure-volume relationship (Figure 1E,G).

Besides the functional alterations, the structural remodelling of the heart also signalled the advanced state of HF pathology. The approximately two-fold greater echocardiography-derived LV mass and heart weight-to-tibial length ratio of TAC-M and TAC-HF groups compared with the sham animals confirmed the development of myocardial hypertrophy (Figure 1B and Figure 2D). Wall thickness parameters (Table 1) and relative wall thickness (Table 1) showed greater increase in the TAC-M groups, suggesting a rather concentric geometry of hypertrophy. In the TAC-HF group however, ventricular dilation was predominant, as demonstrated by the alterations of ventricular diameters and volumes (Table 1). Histological analysis detected significant interstitial myocardial fibrosis in the LV of both TAC groups (Figure 2F,H). Excessive fibrosis was found in the RV of the TAC-HF group as well, while the TAC-M group showed only a tendency towards RV fibrosis (Figure 2G,H). The isolated RV weight-totibial length ratio was also found to be elevated in the TAC-M and TAC-HF groups compared with sham (Figure 2E).

Figure 1 Characterization of the TAC model. Upper panel: morphology and clinical parameters of heart failure. (A) Representative M-mode echocardiographic images at the midpapillary muscle level. (B) Left ventricular mass (LV mass) calculated from echocardiographic data. (C) Ejection fraction (EF) calculated from invasive P-V measurement data. (D) Plasma N-terminal prohormone of brain natriuretic peptide (NT-proBNP) levels measured with ELISA. Lower panel: left ventricular haemodynamic parameters from invasive P-V measurements. (E) Representative original steady-state recordings (top) and loops obtained at different preloads during transient vena cava occlusions (bottom). (F) Systolic parameters—arterial elastance (E_a), slope of end-systolic pressure-volume relationship (ESPVR) and ventriculo-arterial coupling (VAC). (G) Diastolic parameters—left ventricular end-diastolic pressure (LVEDP), slope of end-diastolic pressure-volume relationship (EDPVR) and time constant of left ventricular pressure decay (Tau). Values are means \pm SE. Normal distribution of the data was assessed with Shapiro—Wilk test. One-way analysis of variance (ANOVA) followed by Tukey's post hoc test or Kruskal—Wallis test followed by Dunn's post hoc test were carried out depending on the distribution of the datasets. n = 6 (except for the ESPVR, VAC and EDPVR parameters in the TAC-HF group, where n = 5 due to technical reasons). *P < 0.05 vs. sham; #P < 0.05 vs. TAC-M. ELISA, enzyme-linked immunosorbent assay; HF, heart failure; LVAWT_d, left ventricular anterior wall thickness in diastole; LVEDD, left ventricular end-diastolic diameter; LVPWT_d, left ventricular posterior wall thickness in diastole; TAC, transverse aortic constriction.



Myocardial expression of inflammasome components

In the LV, expression of inflammasome components showed an overall higher tendency in the TAC-HF group (see *Figure 2A,C*). Among the inflammasome sensors, NLR family CARD domain-containing protein 4 (NLRC4) and absent in melanoma 2 (AIM2) were up-regulated compared with the controls. Pro-IL-1 β expression also featured a more than

two-fold elevation in the TAC-HF animals. The most abundant pro-caspase-1 isoform (with 40 kDa molecular weight) was found to be statistically significantly up-regulated as well. None of the changes described above were present in the LV of the TAC-M group, only the expression of GSDMD increased in this group. The inflammasome components in the RV of the TAC-HF rats showed a similar pattern of up-regulation (*Figure 2B,C*). Interestingly, the fold changes were even greater than those of the TAC-HF LV, while the

Table 1 Characterization of the TAC model

	Sham	TAC-M	TAC-HF
n	6	6	6
Body weight, g	532 ± 16	474 ± 22	439 ± 26*
Echocardiographic data			
HR, b.p.m.	384 ± 10	330 ± 7*	301 ± 9*
LVAWTd, mm	1.91 ± 0.05	2.76 ± 0.16 *	2.33 ± 0.20
LVPWTd, mm	2.00 ± 0.09	3.28 ± 0.24 *	3.29 ± 0.29* "
LVESD, mm	4.32 ± 0.26	$5.95 \pm 0.27*$	$7.20 \pm 0.42^{*\#}$
LVEDD, mm	7.55 ± 0.41	8.57 ± 0.21	9.60 ± 0.34 *
FS, %	43 ± 1	31 ± 3	25 ± 3*
RWT	0.53 ± 0.04	0.71 ± 0.04 *	0.59 ± 0.06
Haemodynamic data			
HR, b.p.m.	338 ± 12	302 ± 7*	290 ± 9*
SBP, mmHg	128 ± 8	254 ± 9*	224 ± 13*
DBP, mmHg	97 ± 7	95 ± 7	86 ± 5
MAP, mmHg	107 ± 8	148 ± 6*	132 ± 8
LVESV, μL	125.8 ± 10.7	$208.4 \pm 21.9*$	291.4 ± 26.7* [#]
LVEDV, μL	291.8 ± 21.7	319.5 ± 34.9	369.1 ± 20.6 "
LVESP, mmHg	124.3 ± 8.01	$246.7 \pm 8.73*$	206.0 ± 11.3* [#]
dPdt _{max} , mmHg/s	8652 ± 710.4	8818 ± 547.2	6874 ± 469.0 "
dPdt _{min} , mmHg/s	$-10,564 \pm 1020$	-8547 ± 312.6	-5919 ± 277.7* [#]
SV, μL	166.1 ± 12.9	111.2 ± 18.3	77.72 ± 13.1*
CO, mL/min	55.7 ± 3.67	33.3 ± 5.54*	$22.2 \pm 3.28*$

Values are means ± SE. Normal distribution of the data was assessed with Shapiro–Wilk test. One-way analysis of variance (ANOVA) followed by Tukey's post hoc test or Kruskal–Wallis test followed by Dunn's post hoc test were carried out depending on the distribution of the datasets.

CO, cardiac output; dP/dt_{max} and dP/dt_{min} , maximal slope of the systolic pressure increment and the diastolic pressure decrement; FS, fractional shortening; HR, heart rate; LVAWTd and LVPWTd, left ventricular anterior and posterior wall thickness in diastole; LVESD and LVEDD, left ventricular end-systolic and end-diastolic diameter; LVESP, left ventricular end-systolic pressure; LVESV and LVEDV, left ventricular end-systolic and end-diastolic volume; MAP, mean arterial pressure; n, number of rats; RWT, relative wall thickness; SBP and DBP, systolic and diastolic blood pressure; SV, stroke volume; TAC, transverse aortic constriction.

*P < 0.05 vs. sham.

TAC-M group showed no statistically significant alterations (except for the change in GSDMD expression) in the RV, either. Nuclear factor kappa-light-chain-enhancer of activated B cells (NF-κB), an upstream activator of the inflammasome pathway, was exclusively up-regulated in both ventricles of the TAC-HF animals (*Figure* S1).

TAC-HF group as well. Inflammasome component expressions were practically similar to the controls in the TAC-M group, only AIM2 and pro-IL-1 β showed a tendency towards elevation. Not NF- κ B expression, but its phosphorylation ratio was increased in both TAC groups (*Figure S2*).

Lung tissue changes and inflammasome component expression

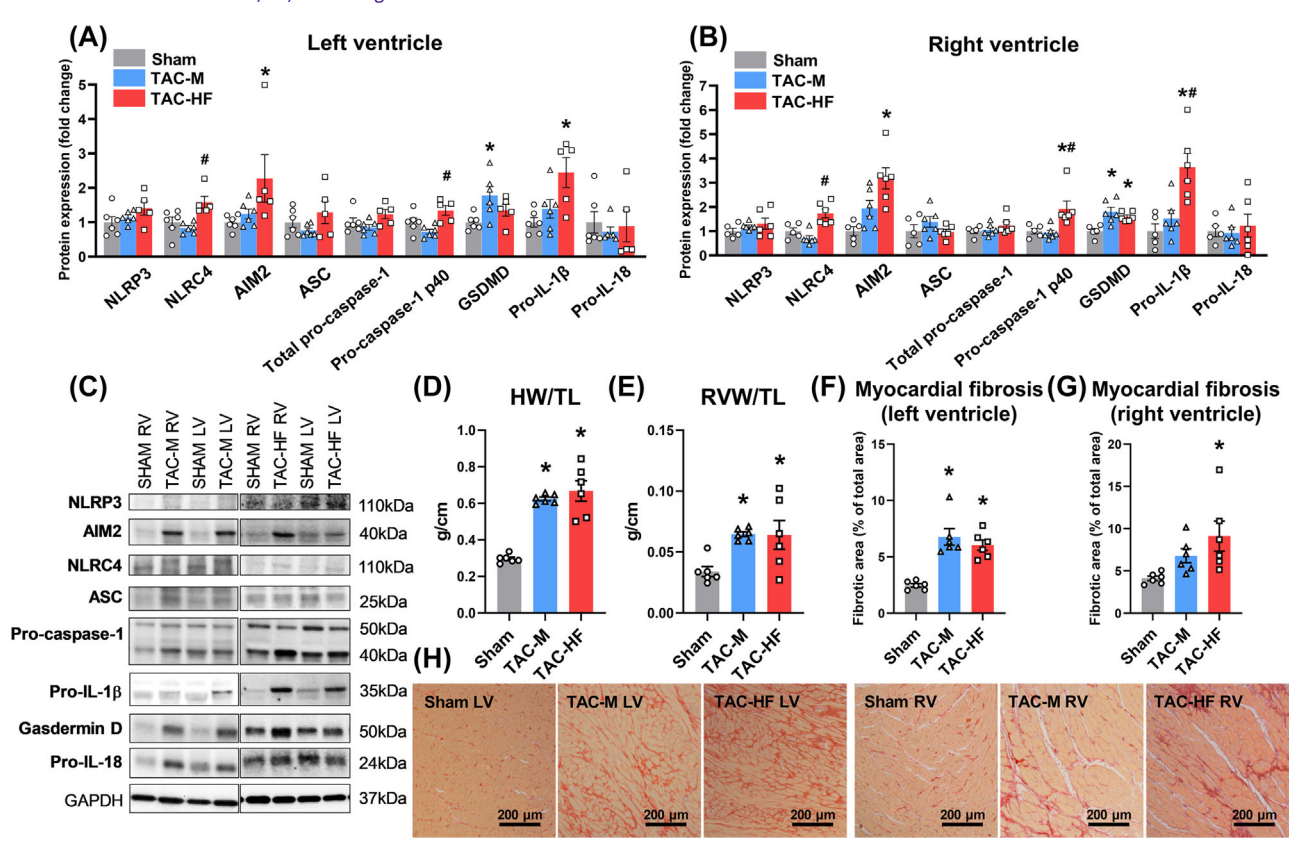
Wet lung weight normalized to tibial length were increased in all of the TAC animals compared with the sham group, indicating pulmonary congestion (*Figure 3E*). Histological analyses detected CD68 + leukocyte infiltration in the lung tissue of the TAC-HF rats (and a strong tendency in the TAC-M group as well), while fibrosis was not found to be significantly different in any of the groups (*Figure 3B,C,F,G*). The expression of certain inflammasome-related proteins was elevated in the lungs of TAC-HF animals as well (*Figure 3A,D*). In contrast to the myocardial findings, NLRP3 expression showed a marked growth along with AIM2, while NLRC4 remained unchanged compared with the controls. In addition, pro-caspase-1 and pro-IL-1β were significantly up-regulated in the

Liver tissue changes and inflammasome component expression

The mean liver weight-to-tibial length ratio was unaltered in the TAC animals (*Figure 4E*). The TAC-HF group showed a tendency towards liver fibrosis and CD68+ infiltration, although not statistically significantly (*Figure 4B,C,F,G*). Plasma albumin was found to be decreased and total bilirubin concentrations elevated in the TAC-HF group, while transaminases displayed no significant changes (*Table 2*). These liver function tests indicate preserved liver parenchyma, and the dominance of congestion (instead of hypoperfusion) in the clinical picture. Interestingly, inflammasomal components were repressed in the liver of TAC-HF animals, while the TAC-M group did not present any meaningful alterations (*Figure 4A,D*).

 $^{^{\#}}P < 0.05 \text{ vs. TAC-M}.$

Figure 2 Myocardial tissue changes. (A, B) Western blot analysis of left and right ventricular major inflammasome component expression levels normalized to GAPDH. (C) Representative images of blots. Heart weight (D) and right ventricle weight (E) normalized to tibial length. (F, G) Left and right ventricular fractional area of interstitial fibrosis. (H) Representative photomicrographs with picrosirius red staining of left and right ventricular myocardium (red colour indicates fibrotic area). $50 \times magnification$, scale bar $200 \ \mu m$. Values are means \pm SE. Normal distribution of the data was assessed with Shapiro–Wilk test. One-way analysis of variance (ANOVA) followed by Tukey's post hoc test or Kruskal–Wallis test followed by Dunn's post hoc test were carried out depending on the distribution of the datasets. n = 6 (except for the Western blot measurements in the LV of the TAC-HF group and the RV of the sham group, where n = 5 due to technical reasons). *P < 0.05 vs. sham; #P < 0.05 vs. TAC-M. AIM2, absent in melanoma 2; ASC, apoptosis-associated speck-like protein containing a CARD; GAPDH, glyceraldehyde-3-phosphate dehydrogenase; GSDMD, gasdermin D; HF, heart failure; HW, heart weight; LV, left ventricle; NLRC4, NLR family CARD domain-containing protein 4; NLRP3, NLR family pyrin domain-containing protein 3; Pro-IL-18, pro-interleukin-18; Pro-IL-1β, pro-interleukin-1 beta; RV, right ventricle; RVW, right ventricle weight; TAC, transverse aortic constriction; TL, tibial length.



Kidney tissue changes and inflammasome component expression

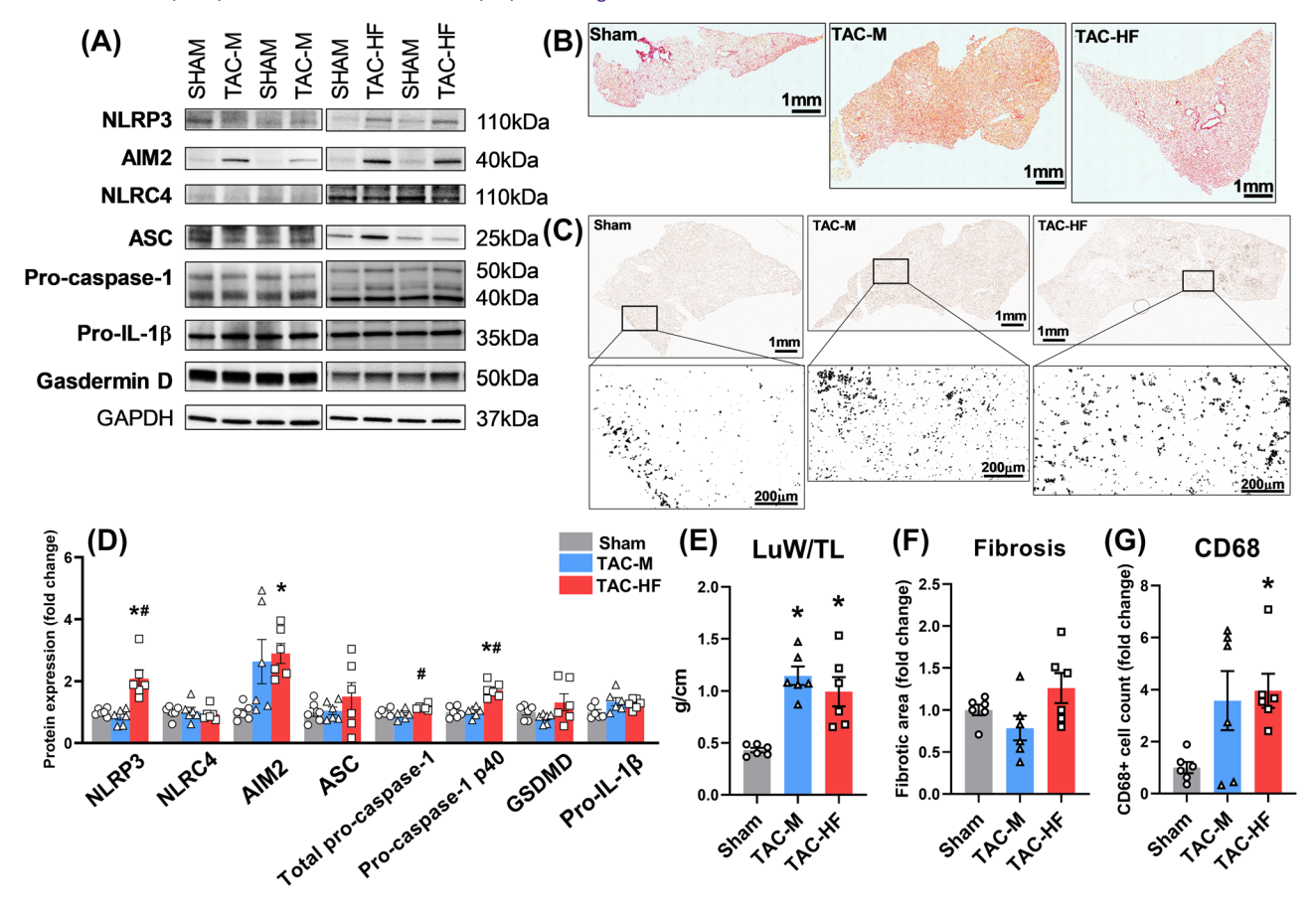
Both TAC groups featured renal atrophy with decreased kidney weights and considerable fibrosis (*Figure 5B,D,E*). The fibrosis in the TAC-HF group differed statistically significantly from both the sham and the TAC-M groups as well. In spite of the described kidney changes, inflammasome component expressions were unchanged in the TAC animals (*Figure 5A,C*).

Discussion

Advanced HF—especially when extracardiac organ dysfunction is already present—is associated with frequent hospital-

izations and high mortality rates, significantly burdening both the healthcare system and the individual patients.²⁹ Haemodynamic disturbances in HF result in various kinds of tissue damage, triggering sterile inflammation across the body.³⁰ Inflammatory mediators exert a detrimental effect on the myocardium and extracardiac organs as well, resulting in a positive feedback loop that undermines the clinical status further. 31,32 Several efforts have already been made to utilize systemic anti-inflammatory therapies in HF, but side effects such as infections or cancer often outweigh the cardiovascular gains. 12,13 Further attempts should specifically target the active inflammatory pathways in HF, not overlooking the end-organs, either. Given the diversity of signals that activate them, inflammasome receptor proteins are ideal candidates of targeted anti-inflammatory therapy.³³ Hence, in the present study, we aimed to gain a better understanding of

Figure 3 Lung tissue changes. Western blot analysis of major inflammasome component expression levels normalized to GAPDH (D) and representative images of blots (A). (B, F) Histological evaluation of relative fibrosis area in lung tissue on picrosirius red-stained sections. Scale bar 1 mm. (C, G) Identification of macrophages in lung tissue by immunohistochemical detection of CD68. Scale bar 1 mm on top and middle images, 200 μm on bottom images. (E) Lung weight normalized to tibial length. Values are means \pm SE. Normal distribution of the data was assessed with Shapiro–Wilk test. One-way analysis of variance (ANOVA) followed by Tukey's post hoc test or Kruskal–Wallis test followed by Dunn's post hoc test were carried out depending on the distribution of the datasets. n = 6 in all groups. *P < 0.05 vs. sham; #P < 0.05 vs. TAC-M. AIM2, absent in melanoma 2; ASC, apoptosis-associated speck-like protein containing a CARD; GAPDH, glyceraldehyde-3-phosphate dehydrogenase; GSDMD, gasdermin D; HF, heart failure; LuW, lung weight; NLRC4, NLR family CARD domain-containing protein 4; NLRP3, NLR family pyrin domain-containing protein 3; Pro-IL-1β, pro-interleukin-1 beta; TAC, transverse aortic constriction; TL, tibial length.

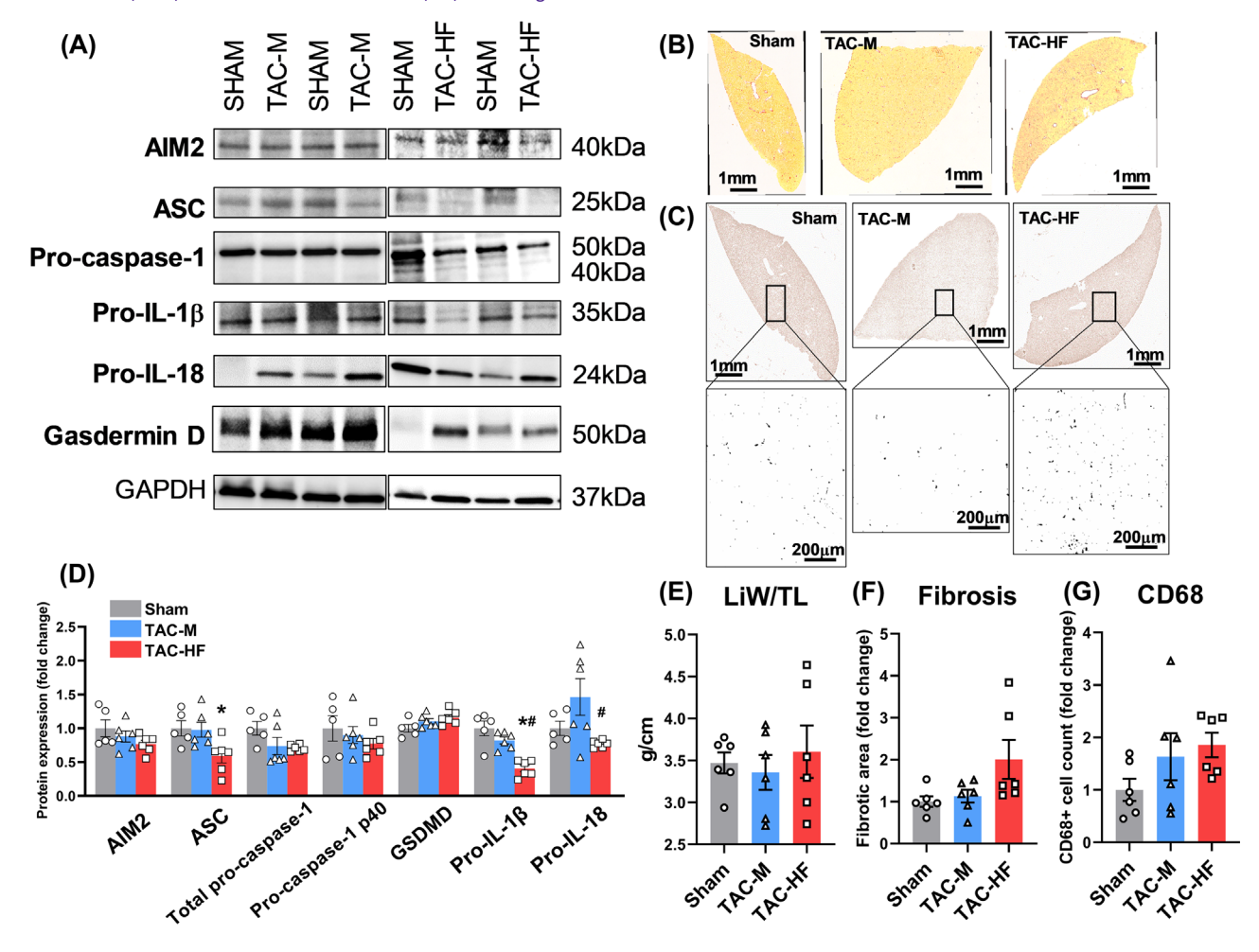


multiorgan inflammasome activation patterns in a small animal model of advanced HF. Since the whole clinical picture, rather than mere cardiac function, was the focus of our investigation, we formed our TAC-HF group based on the presence of clinical signs of severe HF. Another subpopulation of our animals (TAC-M group) developed a milder HF phenotype with evident cardiac remodelling and dysfunction, but without resting symptoms during the same monitoring period.

The role of the NLRP3 inflammasome sensor in HF pathophysiology is well-established, with numerous studies, including a phase 1B clinical trial, exploring its inhibition for therapeutic use. Recent publications have confirmed LV activation of other receptors, such as AIM2 and NLRC4, in HF across both animal models and human patients. Resulting in line with these prior results, we detected the priming of the AIM2 and NLRC4 proteins (but not NLRP3) in the LV tissue

of animals with advanced HF (Figure 2A, Figure S1). Both AIM2 and NLRC4 sensors are activated by pathogen-derived antigens.¹⁷ Although inflammasome priming and activation require different signals, 37 our findings align with the theory of gut microbiome translocation in HF. 38,39 This hypothesis suggests that splanchnic congestion and ischaemia in HF weaken intestinal barriers, allowing bacterial antigens to enter the circulation. 38,39 NLRC4 up-regulation (Figure 2A,B) and cardiac cachexia—a criterion for group selection (see Table S1) and reflected in body weight (Table 1)—were exclusive to the TAC-HF group, indicating that intestinal system disturbances are a feature of advanced HF. Interestingly, none of the inflammasome components were found to be up-regulated in the liver tissue of our TAC animals, even though the liver is the first organ to meet bacterial antigens exiting the gut circulation.

Figure 4 Liver tissue changes. Western blot analysis of major inflammasome component expression levels normalized to GAPDH (D) and representative images of blots (A). (B, F) Histological evaluation of relative fibrosis area in liver tissue on picrosirius red-stained sections. Scale bar 1 mm. (C, G) Identification of macrophages in liver tissue by immunohistochemical detection of CD68. Scale bar 1 mm on top and middle images, 200 μm on bottom images. (E) Liver weight normalized to tibial length. Values are means \pm SE. Normal distribution of the data was assessed with Shapiro–Wilk test. One-way analysis of variance (ANOVA) followed by Tukey's post hoc test or Kruskal–Wallis test followed by Dunn's post hoc test were carried out depending on the distribution of the datasets. n = 6 (except for the Western blot measurements in the sham group where n = 5 due to technical reasons). *P < 0.05 vs. sham; #P < 0.05 vs. TAC-M. AIM2, absent in melanoma 2; ASC, apoptosis-associated speck-like protein containing a CARD; GAPDH, glyceraldehyde-3-phosphate dehydrogenase; GSDMD, gasdermin D; HF, heart failure; LiW, liver weight; Pro-IL-18, pro-interleukin-18; Pro-IL-1β, pro-interleukin-1 beta; TAC, transverse aortic constriction; TL, tibial length.



LV failure results in the eventual impairment of RV through post-capillary pulmonary hypertension (PH).⁴⁰ Although the haemodynamic examination of the pulmonary circulation and the RV was not possible in the current experiment, the detected alterations in both TAC-HF and TAC-M groups (elevated LVEDP, pulmonary congestion and structural RV remodelling, see *Figures 1–3*) were consistent with these mechanisms. Recent studies postulate that inflammation might further damage the pulmonary vasculature and the RV independently of the haemodynamic conditions. Al Qazazi et al. studied multiple preclinical models of PH and concluded that the activation of NLRP3 inflammasomes contributed to the decompensation of RV function in PH.²⁵ Moreover, they discovered opposing polarization of macrophages in the lung

and RV tissue, suggesting the presence of different pathomechanisms in the haemodynamically connected organs. Two other contemporary works employed external stressors to induce inflammation in PH and LV HF animal models, revealing significant RV deterioration as a result. ^{24,41} In line with these results, we found an increased number of CD68+ monocytes/macrophages in the lungs of TAC-HF and TAC-M animals (see *Figure 3G*). However, the priming of the inflammasome pathway was only present in the lung and RV tissue of the clinically progressed TAC-HF group (see *Figures 2* and *3*, *Figures S1* and *S2*). In addition, the expression patterns of the inflammasome receptors were different in the lung and the heart—NLRC4 activation was specific to the myocardium, while NLRP3 was up-regulated only in the

lung. It is also interesting to note that inflammasome expressions were comparable in the two ventricles, even trending towards higher levels in the RV. Taken together, in advanced HF, the lung may be a possible additional source of inflammation, and both ventricles are affected regardless of the location of cardiac damage. The success of previously utilized NLRP3 inhibitor therapies in HF might have depended on

Table 2 Circulating biochemical markers of liver function

	Sham	TAC-M	TAC-HF
n	6	6	6
Albumin, g/L	26.0 ± 0.4	24.6 ± 1.0	$22.7 \pm 0.7*$
AST, IU/L	107 ± 6	113 ± 17	134 ± 10^{a}
ALT, IU/L	55 ± 3	44 ± 4	42 ± 5
Total bilirubin, μmol/L	1.2 ± 0.1	1.1 ± 0.2	$2.5 \pm 0.3*^{\#}$

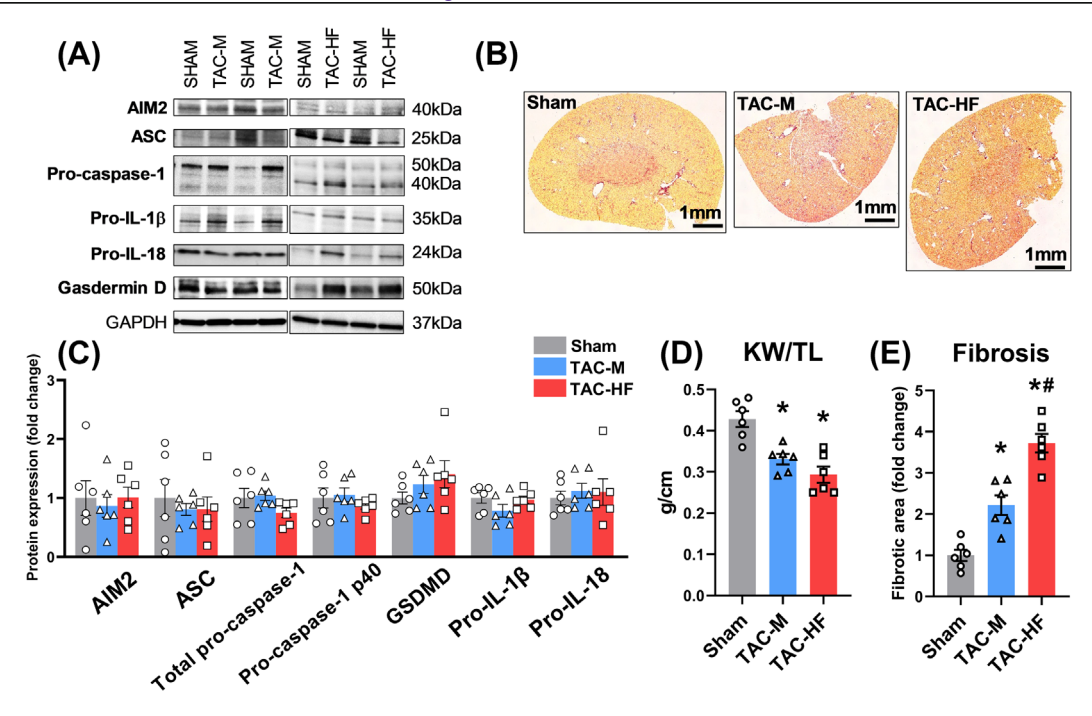
Values are means ± SE. Normal distribution of the data was assessed with Shapiro–Wilk test. One-way analysis of variance (ANOVA) followed by Tukey's post hoc test or Kruskal–Wallis test followed by Dunn's post hoc test were carried out depending on the distribution of the datasets.

ALT, alanine aminotransferase; AST, aspartate aminotransferase; *n*, number of rats; TAC, transverse aortic constriction.

the involvement of pulmonary damage in the clinical picture, while the selective modulation of NLRC4 or AIM2 seems a more promising approach for HF.

The pathological alterations of liver in HF are mainly determined by the presence of hypoperfusion and systemic congestion. 42 The elevation of circulating transaminase levels indicates hypoperfusion, while a cholestatic profile of liver enzymes and hypoalbuminaemia demonstrate congestion.⁴³ Liver function tests in our TAC-HF group suggested the dominance of congestion, which can be the result of the postulated RV dysfunction of these animals. The unchanged liver function of the TAC-M rats is in good agreement with the absence of clinical HF signs. In this context, down-regulation of inflammasomes in the TAC-HF group is puzzling, especially alongside with the elevated CD68+ cell count (Figure 4D,G). None of the measured liver parameters indicate parenchymal cell loss or other disturbances that can account for a relative decrease of protein expression in the TAC-HF group. The histochemical marker CD68 marks either resident Kupffer cells in the liver tissue or infiltrating monocytes/macrophages. 44,45 Both these cell types are known to participate in liver changes associated with HF.46,47 Their ability to express inflammasomes has also been confirmed. 45,48 According to literature data, the up-regulation of inflammasomes is expected

Figure 5 Kidney tissue changes. Western blot analysis of major inflammasome component expression levels normalized to GAPDH (C) and representative images of blots (A). (B, E) Histological evaluation of relative fibrosis area in kidney tissue on picrosirius red-stained sections. Scale bar 1 mm. (D) Kidney weight normalized to tibial length. Values are means ± SE. Normal distribution of the data was assessed with Shapiro–Wilk test. One-way analysis of variance (ANOVA) followed by Tukey's post hoc test or Kruskal–Wallis test followed by Dunn's post hoc test were carried out depending on the distribution of the datasets. n = 6 in all groups. *P < 0.05 vs. sham; #P < 0.05 vs. TAC-M. AIM2, absent in melanoma 2; ASC, apoptosis-associated speck-like protein containing a CARD; GSDMD, gasdermin D; HF, heart failure; KW, kidney weight; Pro-IL-18, pro-interleukin-18; Pro-IL-1β, pro-interleukin-1 beta; TAC, transverse aortic constriction; TL, tibial length.



 $^{^{}a}n = 4$ due to technical reasons.

^{*}P < 0.05 vs. sham.

 $^{^{\#}}P < 0.05 \text{ vs. TAC-M}.$

throughout the spectrum of liver diseases, even in advanced cirrhosis. ^{49,50} Further research is needed to uncover the underlying factors behind these findings.

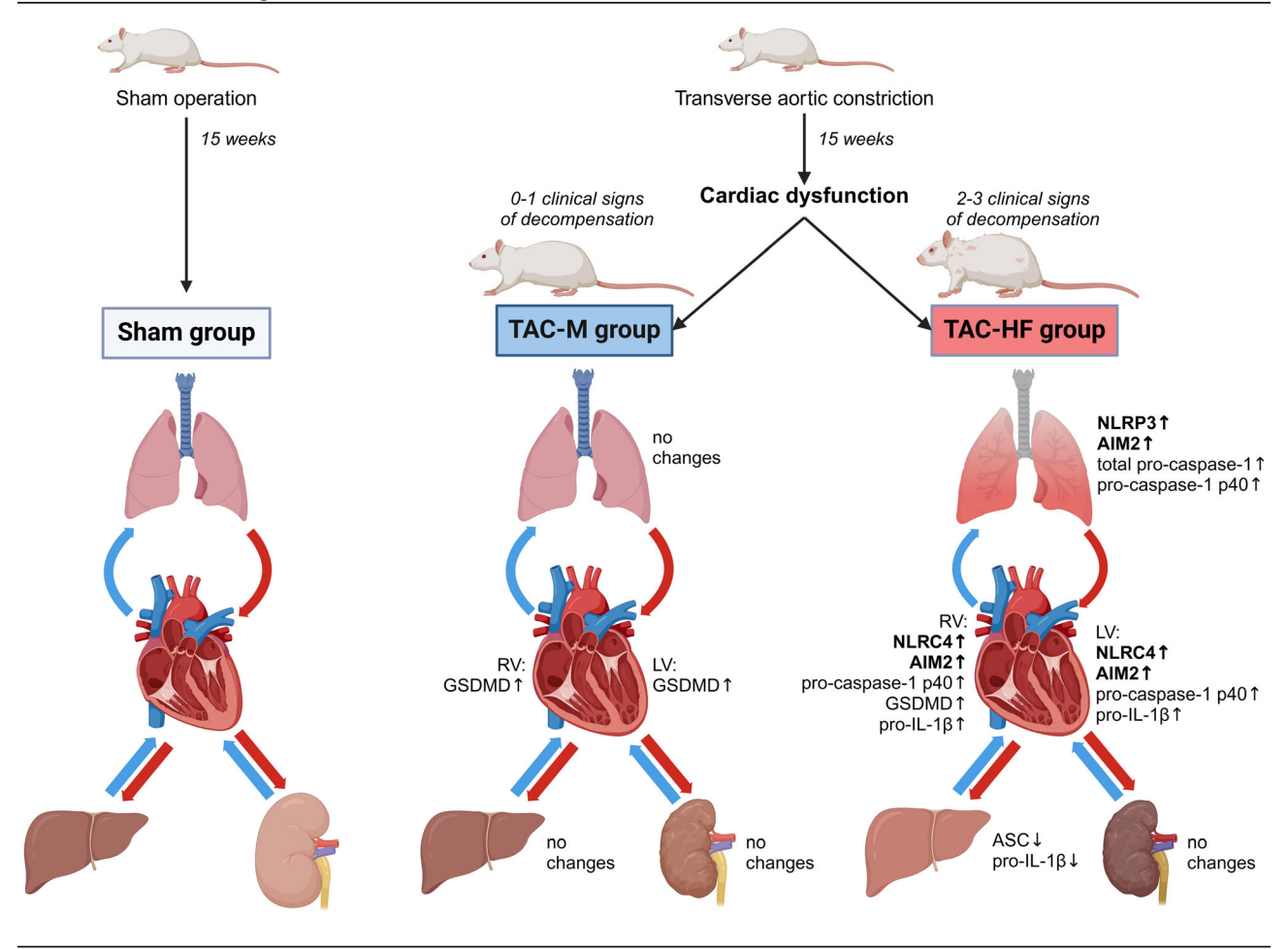
Both of our aortic constricted groups developed kidney atrophy and fibrosis without any changes of the inflammasome components (*Figure 5C–E*). Chronic kidney disease and renal failure patients are known to have elevated levels of circulating inflammatory cytokines, the role of IL-1 β in diseased or fibrotic kidney tissue has also been proven. The is little data about the direct function of inflammasomal proteins in cardiorenal interactions. A functionally intact kidney atrophy without inflammation has already been described in a murine TAC model by Richards et al. The atrophy of kidneys was also discovered in a transgenic mouse model of dilatative cardiomyopathy, where renal fibrosis and elevated inflammatory cytokine levels were identified. However, the expression of IL-1 β was unchanged in this experiment. Taken together, the pathomechanism of kidney tis-

sue damage associated with HF is likely to unfold without the involvement of the inflammasome pathway according to our results.

Our study faces certain limitations. A potential limitation is that we focused on inflammasome priming and did not assess downstream activation markers such as ASC speck formation, cytokine release and protein cleavage. Additionally, while we investigated NF-κB as an upstream regulator of inflammasome components, other potential regulatory pathways were not examined. Future studies should address these aspects to provide a more comprehensive understanding of inflammasome regulation in this context.

In conclusion, we provided the first comprehensive characterization of inflammasome component protein expressions in a small animal model of advanced HF induced by pressure overload in multiple key organs affected by the disease (Figure 6). In line with previous findings, we found the priming of the AIM2 and NLRC4 inflammasome sensors in the LV

Figure 6 Schematic view of the main findings. AIM2, absent in melanoma 2; ASC, apoptosis-associated speck-like protein containing a CARD; GSDMD, gasdermin D; LV, left ventricle; NLRC4, NLR family CARD domain-containing protein 4; NLRP3, NLR family pyrin domain-containing protein 3; Pro-IL-1β, Pro-interleukin-1 beta; RV, right ventricle; TAC, transverse aortic constriction.



myocardium. The RV featured a comparable degree of inflammasome up-regulation, despite the pathological stimulus of our model affecting primarily the LV. We discovered a different pattern of inflammasome expression in the lung, as the AIM2 and NLRP3, but not the NLRC4 inflammasome sensors were up-regulated. Surprisingly, down-regulated inflammasomes in the liver and unchanged expression profile were found in the kidney, despite the histological evidence of typical HF-associated pathological alterations. In a group of similar HF model animals displaying no clinical signs of decompensation, milder cardiac dysfunction and moderate, yet significant organ deviations were measured. The inflammasome changes of the advanced HF group were absent in these compensated animals.

Acknowledgements

We are grateful for the excellent technical assistance of Henriett Biró, Andrea Kovács, Orsolya Szalai and Benjamin Prokaj.

Conflict of interest

Péter Ferdinandy is the founder and CEO of Pharmahungary Group, a group of R&D companies. The other authors have nothing to declare.

Funding

Project no. RRF-2.3.1-21-2022-00003 has been implemented with the support provided by the European Union. TKP2021-EGA-23 has been implemented with the support provided by the Ministry of Innovation and Technology of Hungary from the National Research, Development and Innovation Fund, financed under the TKP2021-EGA funding scheme. The work was supported by the European Union's Horizon 2020 Research and Innovation Programme under grant agreement no. 739593 and by a Momentum Research

Grant from the Hungarian Academy of Sciences (LP-2021-14 to Z.V.V.). The study was supported by a grant from the National Research, Development and Innovation Office (NKFIH) of Hungary (ADVANCED 150829 and K134939 to T. R., STARTING 150923 to M.R. and FK134751 to Z.V.V.). D.N. was further supported by the UNKP-22-3-1 New National Excellence Program of the Ministry for Innovation and Technology from the National Research, Development and Innovation Fund source (ÚNKP-22-3-I-SE-7); M.R. (BO/ 00619/22) and Zs.O. (BO/00012/24/5) were supported by the János Bolyai Research Scholarship of the Hungarian Academy of Sciences, Zs.O. was supported by UNKP-23-4-II-SE-26 from the National Research, Development and Innovation Fund source. D.N. was further supported by the EKÖP-2024-18 grant from the National Development and Innovation Fund.

Supporting information

Additional supporting information may be found online in the Supporting Information section at the end of the article.

Table S1. Clinical signs of the included TAC-operated rats at the end of the follow-up period.

Table S2. List of antibodies used for Western blot analysis. **Figure S1.** Protein expression and phosphorylation of nuclear factor kappa-light-chain-enhancer of activated B cells in the heart and representative images of blots. NF- κ B, nuclear factor kappa-light-chain-enhancer of activated B cells; TAC, transverse aortic constriction; pNF- κ B, phosphorylated NF- κ B; GAPDH, glyceraldehyde-3-phosphate dehydrogenase.

Figure S2. Protein expression and phosphorylation of nuclear factor kappa-light-chain-enhancer of activated B cells in the lung and representative images of blots. NF-κB, nuclear factor kappa-light-chain-enhancer of activated B cells; TAC, transverse aortic constriction; pNF-κB, phosphorylated NF-κB; GAPDH, glyceraldehyde-3-phosphate dehydrogenase.

Data S1. Supplementary Information.

References

- Savarese G, Becher PM, Lund LH, Seferovic P, Rosano GMC, Coats AJS. Global burden of heart failure: a comprehensive and updated review of epidemiology. Cardiovasc Res 2023;118: 3272-3287. doi:10.1093/cvr/cvac013
- 2. Fang JC, Ewald GA, Allen LA, Butler J, Westlake Canary CA, Colvin-Adams M,
- et al. Advanced (stage D) heart failure: a statement from the Heart Failure Society of America Guidelines Committee. *J Card Fail* 2015;**21**:519-534. doi:10.1016/j.cardfail.2015.04.013
- 3. Guglin M, Zucker MJ, Borlaug BA, Breen E, Cleveland J, Johnson MR, *et al.* Evaluation for heart transplantation
- and LVAD implantation: JACC council perspectives. *J Am Coll Cardiol* 2020; **75**:1471-1487. doi:10.1016/j.jacc.2020. 01.034
- 4. Hong KN, Iribarne A, Worku B, Takayama H, Gelijns AC, Naka Y, et al. Who is the high-risk recipient? Predicting mortality after heart transplant using

pretransplant donor and recipient risk factors. *Ann Thorac Surg* 2011;**92**: 520-527; discussion 7. doi:10.1016/j. athoracsur.2011.02.086

- Ciccarelli M, Dawson D, Falcao-Pires I, Giacca M, Hamdani N, Heymans S, et al. Reciprocal organ interactions during heart failure: a position paper from the ESC Working Group on Myocardial Function. Cardiovasc Res 2021;117: 2416-2433. doi:10.1093/cvr/cvab009
- Hartupee J, Mann DL. Neurohormonal activation in heart failure with reduced ejection fraction. *Nat Rev Cardiol* 2017; 14:30-38. doi:10.1038/nrcardio.2016. 163
- Vasan RS, Sullivan LM, Roubenoff R, Dinarello CA, Harris T, Benjamin EJ, et al. Inflammatory markers and risk of heart failure in elderly subjects without prior myocardial infarction: the Framingham Heart Study. Circulation 2003;107:1486-1491. doi:10.1161/01. cir.0000057810.48709.f6
- Adamo L, Rocha-Resende C, Prabhu SD, Mann DL. Reappraising the role of inflammation in heart failure. *Nat Rev Cardiol* 2020;17:269-285. doi:10.1038/ s41569-019-0315-x
- 9. Murphy SP, Kakkar R, McCarthy CP, Januzzi JL Jr. Inflammation in heart failure: JACC state-of-the-art review. *J Am Coll Cardiol* 2020;75:1324-1340. doi:10.1016/j.jacc.2020.01.014
- Brower GL, Janicki JS. Pharmacologic inhibition of mast cell degranulation prevents left ventricular remodeling induced by chronic volume overload in rats. *J Card Fail* 2005;11:548-556. doi:10.1016/j.cardfail.2005.05.005
- Chung ES, Packer M, Lo KH, Fasanmade AA, Willerson JT, Anti TNFTACHFI. Randomized, double-blind, placebo-controlled, pilot trial of infliximab, a chimeric monoclonal antibody to tumor necrosis factor-alpha, in patients with moderate-to-severe heart failure: results of the anti-TNF Therapy Against Congestive Heart Failure (ATTACH) trial. Circulation 2003;107:3133-3140. doi:10.1161/01.CIR.0000077913.60364.
- Mann DL, McMurray JJ, Packer M, Swedberg K, Borer JS, Colucci WS, et al. Targeted anticytokine therapy in patients with chronic heart failure: results of the Randomized Etanercept Worldwide Evaluation (RENEWAL). Circulation 2004;109:1594-1602. doi:10.1161/ 01.CIR.0000124490.27666.B2
- Ridker PM, Everett BM, Thuren T, MacFadyen JG, Chang WH, Ballantyne C, et al. Antiinflammatory therapy with canakinumab for atherosclerotic disease. N Engl J Med 2017;377:1119-1131. doi:10.1056/NEJMoa1707914
- 14. Trankle CR, Canada JM, Cei L, Abouzaki N, Oddi-Erdle C, Kadariya D, *et al*. Usefulness of canakinumab to improve exercise capacity in patients with long-term systolic heart failure and elevated C-reactive protein. *Am J Cardiol* 2018;**122**:

- 1366-1370. doi:10.1016/j.amjcard.2018. 07.002
- Everett BM, Cornel JH, Lainscak M, Anker SD, Abbate A, Thuren T, et al. Anti-inflammatory therapy with canakinumab for the prevention of hospitalization for heart failure. Circulation 2019;139:1289-1299. doi:10.1161/ CIRCULATIONAHA.118.038010
- Martinon F, Burns K, Tschopp J. The inflammasome: a molecular platform triggering activation of inflammatory caspases and processing of proIL-beta. Mol Cell 2002;10:417-426. doi:10.1016/s1097-2765(02)00599-3
- Broz P, Dixit VM. Inflammasomes: mechanism of assembly, regulation and signalling. Nat Rev Immunol 2016;16: 407-420. doi:10.1038/nri.2016.58
- Wang Y, Wu Y, Chen J, Zhao S, Li H. Pirfenidone attenuates cardiac fibrosis in a mouse model of TAC-induced left ventricular remodeling by suppressing NLRP3 inflammasome formation. *Cardiology* 2013;126:1-11. doi:10.1159/ 000351179
- Gao R, Shi H, Chang S, Gao Y, Li X, Lv C, et al. The selective NLRP3-inflamma-some inhibitor MCC950 reduces myocardial fibrosis and improves cardiac remodeling in a mouse model of myocardial infarction. *Int Immunopharmacol* 2019; 74:105575. doi:10.1016/j.intimp.2019.04.022
- Wohlford GF, Van Tassell BW, Billingsley HE, Kadariya D, Canada JM, Carbone S, et al. Phase 1B, randomized, double-blinded, dose escalation, single-center, repeat dose safety and pharmacodynamics study of the oral NLRP3 inhibitor dapansutrile in subjects with NYHA II-III systolic heart failure. J Cardiovasc Pharmacol 2020;77:49-60. doi:10.1097/FJC.00000000000000931
- Szabo G, Petrasek J. Inflammasome activation and function in liver disease. Nat Rev Gastroenterol Hepatol 2015;12: 387-400. doi:10.1038/nrgastro.2015.94
- Hutton HL, Ooi JD, Holdsworth SR, Kitching AR. The NLRP3 inflammasome in kidney disease and autoimmunity. Nephrology (Carlton) 2016;21:736-744. doi:10.1111/nep.12785
- Bugyei-Twum A, Abadeh A, Thai K, Zhang Y, Mitchell M, Kabir G, et al. Suppression of NLRP3 inflammasome activation ameliorates chronic kidney disease-induced cardiac fibrosis and diastolic dysfunction. Sci Rep 2016;6: 39551. doi:10.1038/srep39551
- 44. Guo L, Qin G, Cao Y, Yang Y, Dai S, Wang L, et al. Regulation of the immune microenvironment by an NLRP3 inhibitor contributes to attenuation of acute right ventricular failure in rats with pulmonary arterial hypertension. J Inflamm Res 2021;14:5699-5711. doi:10.2147/ JIR.S336964
- Al-Qazazi R, Lima PDA, Prisco SZ, Potus F, Dasgupta A, Chen KH, et al. Macrophage-NLRP3 activation promotes right ventricle failure in pulmonary arterial

- hypertension. *Am J Respir Crit Care Med* 2022;**206**:608-624. doi:10.1164/rccm.202110-2274OC
- Ruppert M, Lakatos BK, Braun S, Tokodi M, Karime C, Olah A, et al. Longitudinal strain reflects ventriculoarterial coupling rather than mere contractility in rat models of hemodynamic overload-induced heart failure. J Am Soc Echocardiogr 2020;33:1264-1275 e4. doi:10.1016/j.echo.2020.05.017
- 27. Ruppert M, Korkmaz-Icoz S, Li S, Nemeth BT, Hegedus P, Brlecic P, et al. Myocardial reverse remodeling after pressure unloading is associated with maintained cardiac mechanoenergetics in a rat model of left ventricular hypertrophy. Am J Physiol Heart Circ Physiol 2016;311:H592-H603. doi:10.1152/ajpheart.00085.2016
- 28. Onodi Z, Ruppert M, Kucsera D, Sayour AA, Toth VE, Koncsos G, et al. AIM2-driven inflammasome activation in heart failure. Cardiovasc Res 2021;117: 2639-2651. doi:10.1093/cvr/cvab202
- Nieminen MS, Dickstein K, Fonseca C, Serrano JM, Parissis J, Fedele F, et al. The patient perspective: quality of life in advanced heart failure with frequent hospitalisations. Int J Cardiol 2015;191: 256-264. doi:10.1016/j.ijcard.2015.04. 235
- Nakayama H, Otsu K. Translation of hemodynamic stress to sterile inflammation in the heart. *Trends Endocrinol Metab* 2013;24:546-553. doi:10.1016/j.tem.2013.06.004
- Boyd JH, Mathur S, Wang Y, Bateman RM, Walley KR. Toll-like receptor stimulation in cardiomyoctes decreases contractility and initiates an NF-kappaB dependent inflammatory response. Cardiovasc Res 2006;72:384-393. doi:10.1016/j.cardiores.2006.09.011
- Matyas C, Erdelyi K, Trojnar E, Zhao S, Varga ZV, Paloczi J, et al. Interplay of liver-heart inflammatory axis and cannabinoid 2 receptor signaling in an experimental model of hepatic cardiomyopathy. Hepatology 2020;71:1391-1407. doi:10.1002/hep.30916
- Chauhan D, Vande Walle L, Lamkanfi M. Therapeutic modulation of inflammasome pathways. *Immunol Rev* 2020; 297:123-138. doi:10.1111/imr.12908
- 34. Cheng X, Zhao H, Wen X, Li G, Guo S, Zhang D. NLRP3-inflammasome inhibition by MCC950 attenuates cardiac and pulmonary artery remodelling in heart failure with preserved ejection fraction. *Life Sci* 2023;333:122185. doi:10.1016/j.lfs.2023.122185
- Durga Devi T, Babu M, Makinen P, Kaikkonen MU, Heinaniemi M, Laakso H, et al. Aggravated postinfarct heart failure in type 2 diabetes is associated with impaired mitophagy and exaggerated inflammasome activation. Am J Pathol 2017; 187:2659-2673. doi:10.1016/j.ajpath.2017.08.023
- 36. Wang X, Pan J, Liu H, Zhang M, Liu D, Lu L, *et al*. AIM2 gene silencing attenu-

- ates diabetic cardiomyopathy in type 2 diabetic rat model. *Life Sci* 2019;**221**: 249-258. doi:10.1016/j.lfs.2019.02.035
- Liao Y, Kong Y, Chen H, Xia J, Zhao J, Zhou Y. Unraveling the priming phase of NLRP3 inflammasome activation: molecular insights and clinical relevance. *Int Immunopharmacol* 2025;146:113821. doi:10.1016/j.intimp.2024.113821
- 38. Krack A, Sharma R, Figulla HR, Anker SD. The importance of the gastrointestinal system in the pathogenesis of heart failure. *Eur Heart J* 2005;**26**:2368-2374. doi:10.1093/eurheartj/ehi389
- Tang WHW, Li DY, Hazen SL. Dietary metabolism, the gut microbiome, and heart failure. Nat Rev Cardiol 2019;16: 137-154. doi:10.1038/s41569-018-0108-7
- Obokata M, Reddy YNV, Melenovsky V, Pislaru S, Borlaug BA. Deterioration in right ventricular structure and function over time in patients with heart failure and preserved ejection fraction. *Eur Heart J* 2019;40:689-697. doi:10.1093/ eurhearti/ehv809
- 41. Yue W, Tong L, Liu X, Weng X, Chen X, Wang D, et al. Short term Pm2.5 exposure caused a robust lung inflammation, vascular remodeling, and exacerbated transition from left ventricular failure to right ventricular hypertrophy. Redox Biol 2019;22:101161. doi:10.1016/j.redox.2019.101161
- Giallourakis CC, Rosenberg PM, Friedman LS. The liver in heart failure. Clin Liver Dis 2002;6:947-967, viii-ix. doi:10.1016/s1089-3261(02)00056-9
- 43. van Deursen VM, Damman K, Hillege HL, van Beek AP, van Veldhuisen DJ,

- Voors AA. Abnormal liver function in relation to hemodynamic profile in heart failure patients. *J Card Fail* 2010;**16**: 84-90. doi:10.1016/j.cardfail.2009.08. 002
- 44. Ju C, Tacke F. Hepatic macrophages in homeostasis and liver diseases: from pathogenesis to novel therapeutic strategies. *Cell Mol Immunol* 2016;13: 316-327. doi:10.1038/cmi.2015.104
- 45. Liu C, Tao Q, Sun M, Wu JZ, Yang W, Jian P, et al. Kupffer cells are associated with apoptosis, inflammation and fibrotic effects in hepatic fibrosis in rats. Lab Invest 2010;90:1805-1816. doi:10.1038/labinvest.2010.123
- Valentova M, von Haehling S, Doehner W, Murin J, Anker SD, Sandek A. Liver dysfunction and its nutritional implications in heart failure. *Nutrition* 2013; 29:370-378. doi:10.1016/j.nut.2012.06.
- Boaru SG, Borkham-Kamphorst E, Tihaa L, Haas U, Weiskirchen R. Expression analysis of inflammasomes in experimental models of inflammatory and fibrotic liver disease. *J Inflamm (Lond)* 2012;9:49. doi:10.1186/1476-9255-9-49
- Kim HY, Kim SJ, Lee SM. Activation of NLRP3 and AIM2 inflammasomes in Kupffer cells in hepatic ischemia/reperfusion. FEBS J 2015;282:259-270. doi:10.1111/febs.13123
- Ma X, Zheng X, Pan L, Zhang X. NLRP3 inflammasome activation in liver cirrhotic patients. *Biochem Biophys Res Commun* 2018;505:40-44. doi:10.1016/ i.bbrc.2018.09.055
- 50. Lozano-Ruiz B, Bachiller V, Garcia-Martinez I, Zapater P, Gomez-Hurtado I,

- Moratalla A, *et al.* Absent in melanoma 2 triggers a heightened inflammasome response in ascitic fluid macrophages of patients with cirrhosis. *J Hepatol* 2015; 62:64-71. doi:10.1016/j.jhep.2014.08.027
- 51. Vesey DA, Cheung C, Cuttle L, Endre Z, Gobe G, Johnson DW. Interleukin-1beta stimulates human renal fibroblast proliferation and matrix protein production by means of a transforming growth factor-beta-dependent mechanism. *J Lab Clin Med* 2002;140:342-350. doi:10.1067/mlc.2002.128468
- 52. Pereira BJ, Shapiro L, King AJ, Falagas ME, Strom JA, Dinarello CA. Plasma levels of IL-1 beta, TNF alpha and their specific inhibitors in undialyzed chronic renal failure, CAPD and hemodialysis patients. *Kidney Int* 1994;45:890-896. doi:10.1038/ki.1994.117
- Zannad F, Rossignol P. Cardiorenal syndrome revisited. *Circulation* 2018;138: 929-944. doi:10.1161/CIRCULATION-AHA.117.028814
- 54. Richards DA, Aronovitz MJ, Calamaras TD, Tam K, Martin GL, Liu P, et al. Distinct phenotypes induced by three degrees of transverse aortic constriction in mice. Sci Rep 2019;9:5844. doi:10.1038/s41598-019-42209-7
- 55. Giam B, Chu PY, Kuruppu S, Smith AI, Horlock D, Murali A, *et al.* Serelaxin attenuates renal inflammation and fibrosis in a mouse model of dilated cardiomyopathy. *Exp Physiol* 2018;**103**: 1593-1602. doi:10.1113/EP087189